Journal of Hydrology 614 (2022) 128539

Contents lists available at ScienceDirect

Journal of Hydrology

journal homepage: www.elsevier.com/locate/jhydrol

Research papers

A computationally efficient hydrologic modeling framework to simulate surface-subsurface hydrological processes at the hillslope scale

Lin Chen [a,*], Jiří Šimůnek [a], Scott A. Bradford [b], Hoori Ajami [a], Menberu B. Meles [b]

[a] Department of Environmental Sciences, University of California, Riverside, CA 92521, USA
[b] USDA, ARS, Sustainable Agricultural Water Systems Unit, Davis, CA 95616, USA

ARTICLE INFO

This manuscript was handled by Corrado Corradini, Editor-in-Chief, with the assistance of Philip Brunner, Associate Editor

Keywords:
Hydrologic model
Computational efficiency
Surface runoff
Vadose zone flow
Water balance
Surface/subsurface interactions

ABSTRACT

Considering surface and subsurface interactions is imperative to predict water movement, water quantity and quality in the environment. However, substantial execution time and over-parameterization presently limit the applicability of integrated hydrologic models at larger scales. Herein, a new efficient coupling routine for one-dimensional (1D) surface–subsurface modeling was developed by externally coupling two widely used open-source codes. KINEROS2 (K2) solves the 1D kinematic wave equation for overland flow, and HYDRUS-1D (H1D) solves the Richards equation for subsurface flow. A novel approach, combined with water balance and boundary condition switching, is used to account for surface ponding and water exchange between the two model domains. A weighting factor related to the surface water depth is used to assign the time series of exchange fluxes in one H1D profile to multiple surface nodes in the K2 calculation. This novel approach enables us to represent the entire subsurface below each overland-flow plane by one vertical soil column with different soil layering. When soil properties vary horizontally, multiple soil columns can represent spatial heterogeneities. The performance of the coupled H1D-K2 model is examined by comparing simulation results with the HYDRUS-2D (H2D) model for six benchmark problems. The solution's robustness, stability, and accuracy are assessed for a wide variety of cases, including multiple rainstorms, different slopes, heterogeneous subsurface, and different bottom boundary conditions resulting in 41 cases. The simulated hydrographs, surface water levels, and water balance components are all in good agreement. Relative mass balance errors are very small, typically not exceeding 4.0% for the coupled H1D-K2 model. Compared with the H2D model, the coupled model achieves a factor of 1.3–10 speedup by applying one H1D soil profile to an entire overland flow plane rather than to individual surface nodes.

1. Introduction

Global water demands for industrial, domestic, and agricultural users have increased by 600 % over the past century due to population growth and economic development (UN World Water Development Report, 2018). Climate change and anthropogenic activities have also influenced water quantity and quality (Haddeland et al., 2014). For example, climate change shifts precipitation patterns and increases the frequency of flooding and droughts (Vorosmarty et al., 2000). Managed aquifer recharge is a promising adaptation measure to reduce water vulnerability and maintain its sustainability (Niswonger et al., 2017, Sasidharan et al., 2018, Marwaha et al., 2021). This water management approach can maximize water storage in groundwater aquifers and increase water supply during droughts (Niswonger et al., 2017, Kourakos et al., 2019). However, there are limitations in available modeling resources for exploring integrated flow processes and impacts associated with managed aquifer recharge programs, climate change, etc. It is imperative to understand surface and subsurface water flow interactions to improve sustainable water resource management (Smith et al., 2004, Fan et al., 2019).

A large number of models have been developed to predict the hydrologic behavior of coupled surface and subsurface systems in response to human activity and climate variability (Woolhiser et al., 1970, Freeze, 1972, Smith and Hebbert, 1983, Qu and Duffy, 2007). These hydrologic models can be divided into four broad categories: empirical models, lumped conceptual models, semi-distributed models (e.g., AGWA/KINEROS2, SWAT), and physically-based distributed models (e.g., HYDRUS (2D/3D), HydroGeoSphere, MIKE SHE, ParFlow-CLM, PIHM,

* Corresponding author at: Department of Environmental Sciences, University of California, Riverside, USA.
E-mail address: linc@ucr.edu (L. Chen).

https://doi.org/10.1016/j.jhydrol.2022.128539
Received 8 July 2022; Received in revised form 14 September 2022; Accepted 23 September 2022
Available online 1 November 2022

WASH123D) (Smith et al., 2004, Goodrich et al., 2012, Lawrence et al., 2019, Liggett et al., 2012, Orth et al., 2015, Šimůnek, 2015, Kollet et al., 2017, Fan et al., 2019). In comparison to empirical and lumped models, physically-based distributed hydrologic models are valuable tools for considering the full complexity of governing physiochemical processes (Singh and Woolhiser, 2002, Smith et al., 2004, Fatichi et al., 2016) and are capable of predicting the spatial and temporal distribution of water flow and pollutant transport at hillslope to watershed scales (Šimůnek, 2015, Kollet et al., 2017, Wen et al., 2021).

Benchmark simulation cases, ranging from simple homogenous cases with constant rainfall rates to more complex cases with subsurface heterogeneity and lateral flow, have been utilized to compare the performance of different physically-based distributed coupled/integrated hydrologic models (Sulis et al., 2010, Smith et al., 2012, Maxwell et al., 2014, Kollet et al., 2017). Results illustrate that all models can reproduce general hydrologic behaviors of benchmark cases (Liggett et al., 2012, Maxwell et al., 2014, Kollet et al., 2017, Wen et al., 2021). However, fully integrated hydrologic models are computationally intensive, require extensive parameterization, and need substantial execution time. These limitations restrict their applicability at large scales.

The surface–subsurface coupling strategy determines the volume and rate of exchange of water between the two domains (Huang and Yeh, 2009), alters the rainfall-runoff behavior, such as peak flow and the onset of water ponding (Kollet et al., 2017), and eventually affects the accuracy, stability, and robustness of a hydrologic model (Liggett et al., 2012, Coon et al., 2020) because of the faster dynamics of surface flow compared to subsurface flow. Coupling strategies are broadly classified into three categories: continuous pressure, first-order exchange (i.e., the exchange flux is determined by a calibrated coefficient and the head difference between the surface and subsurface nodes), and hybrid approaches (e.g., boundary condition (BC) switching, and regularization/penalty methods) (Huang and Yeh, 2009, Coon et al., 2020).

The continuous pressure approach enforces pressure continuity in the two domains (Kollet and Maxwell, 2006), but rapid changes in surface pressure can cause numerical instabilities at the subsurface boundary (Huang and Yeh, 2009, Liggett et al., 2012, De Maet et al., 2015). The convergence is especially poor near the transition from dry surface to surface ponding (Coon et al., 2020). In addition, the same time step must be used for solving the surface and subsurface equations simultaneously, which greatly increases the associated computational cost because smaller time steps are required for surface water flow (Huang and Yeh, 2009, De Maet et al., 2015).

In contrast, a conceptual interface is considered to represent the connectivity between the surface and subsurface in the first-order exchange approach (i.e., Ebel et al., 2009, Liggett et al., 2012). This coupling approach allows surface and subsurface equations to be solved separately (Panday and Huyakorn, 2004), and the exchange water flux through the interface layer is obtained as the product of the pressure difference in the two domains and an exchange coefficient (Qu and Duffy, 2007, Liggett et al., 2012). A properly calibrated exchange coefficient can enhance the solver convergence and produce similar results to the pressure continuity approach (Liggett et al., 2012).

The BC switching approach calculates infiltration rates for stages with and without surface ponding (Camporese et al., 2010, Camporese et al., 2014). The subsurface flow equation is first solved for the atmosphere-controlled BC (i.e., specified time-dependent water fluxes), and then a mass balance calculation is performed to determine the ponding condition at each surface node. Once surface ponding occurs, the land surface BC is switched from an atmospheric-controlled BC to a soil-controlled BC (i.e., specified time-dependent pressure) (Sulis et al., 2010). The BC switching approach causes a time lag between surface and subsurface flows on an overland plane, influencing the onset of runoff generation and the movement of the saturation front when inflow occurs uphill (Sulis et al., 2010).

De Maet et al. (2015) introduced a hybrid coupling approach that combines the continuous pressure and first-order exchange approaches. This hybrid coupling approach can produce similar results to the first-order exchange approaches and improve the scheme's robustness. Although current coupled/integrated hydrologic models reproduce similar hydrographs (Huang and Yeh, 2009, Kollet et al., 2017, Coon et al., 2020), the impact of coupling approaches has not been extensively examined under the complex boundary conditions that occur during multiple rainstorms.

Furthermore, the application of existing coupled models to large-scale problems is limited due to simplified representation of the subsurface and empirical formulations for infiltration estimation (Giráldez and Woolhiser, 1996, Singh and Bhallamudi, 1998) or high computational burden (Morita and Yen, 2002). The computational burden is a significant obstacle that limits the implementation of hydrological models at larger scales. The numerical solution of the Richards equation usually requires fine spatial grids and small time steps, which greatly increase the computation cost (Niswonger et al., 2006; Šimůnek et al., 2006). Small time steps are required to overcome numerical instabilities at the subsurface boundary due to rapid changes in surface pressure (Huang and Yeh, 2009, Liggett et al., 2012). Much effort has been devoted to improving the computational efficiency of integrated hydrologic models, including parallel computing (Kollet and Maxwell, 2006, Brunner and Simmons, 2012), automatically adjusting time step size (Panday and Huyakorn, 2004, Simunek et al., 2005, Sulis et al., 2010, Goodrich et al., 2012), nested discretization (Wang et al., 2018), and dimensionality reduction (Niswonger et al., 2006, Seo et al., 2007, Brunetti et al., 2018). Different (for overland and subsurface flow) and automatically adjusted time steps can significantly enhance the computational efficiency and robustness of the coupled models (Roberts 2003, Simuunek et al., 2005, Goodrich et al., 2012).

Alternatively, dimensionality reduction of the surface and subsurface flow domain can provide a comparative advantage. As unsaturated flow is predominantly vertical (Mantoglou 1992), a single or multiple vertical soil profiles representing one-dimensional (1D) water flow in the vadose zone can be coupled to a 1D overland flow plane. This simplification and dimensionality reduction could reduce computational time compared to variably saturated flow simulations in 2D or 3D (Panday and Huyakorn, 2004, Niswonger et al., 2006, Seo et al., 2007). Several conjunctive surface/subsurface models have been developed to simulate the overland flow on a plane with 1D or 2D overland flow and 1D, 2D, or 3D flow in the vadose zone (Smith and Woolhiser, 1971, Abbott et al., 1986, Singh and Bhallamudi, 1998, Morita and Yen 2002, Panday and Huyakorn, 2004, Thompson et al., 2004, He et al., 2008). Large-scale coupled hydrologic models, such as MIKE SHE (Thompson et al., 2004) and MODFLOW2000-H1D (Seo et al., 2007, Beegum et al., 2018) are examples of this dimensionality reduction approach.

The general objective of this study is to develop a simple, accurate, and computationally efficient coupled hydrologic model for overland flow and variably saturated flow through the vadose zone at the hillslope scale. Two existing open-source 1D codes are coupled for this purpose: KINEROS2 (referred to below as K2) (Smith et al., 1999, Goodrich et al., 2012) for overland flow and HYDRUS-1D (referred to below as H1D) (Simunek et al., 2016) for vertical water flow in the vadose zone. The specific objectives are (i) to develop a novel coupled H1D-K2 model to reduce the dimensionality of the problem and improve the computational efficiency; (ii) to evaluate the robustness of the proposed model by comparing its results with the two-dimensional version of HYDRUS (2D/3D) (referred to below as H2D) on six benchmark problems; and (iii) to investigate the roles of a rainstorm size and frequency, slope, bottom BC, and soil heterogeneity on the surface and subsurface water flow. We pose the following hypotheses: (i) the coupled H1D-K2 model accurately represents the surface–subsurface water flow in response to multiple rainfall storms compared to H2D; (ii) computational time can be reduced by applying one H1D soil profile to an overland flow plane rather than to each individual surface node; and (iii) subsurface heterogeneity and bottom BC affect the runoff

generation mechanism, pattern, and magnitude, while the slope magnitude impacts the timing of the hydrograph and volume of cumulative runoff.

2. Hydrologic models and setups

To achieve these objectives, a novel approach was developed to externally couple two well-established and widely used open-source codes to simulate hydrologic processes at the surface and in the subsurface using a MATLAB (R2021b) script. The K2 model simulates 1D overland flow via the kinematic wave equation (Goodrich et al., 2006), and H1D simulates 1D variably saturated flow in the subsurface (Simunek et al., 2005, Simunek et al., 2016). To evaluate the model performance, we compared the simulation results of the H1D-K2 model with the H2D model that includes an overland flow routine (Šimunek, 2003, Simunek, 2015). The H2D model outputs are used as a reference for model comparison because the model is physically based (solves the Richards and kinematic wave equations simultaneously) and does not reduce the problem's dimensionality (contrary to the coupled H1D-K2 model). The conceptual models for H2D and coupled H1D-K2 are presented in Fig. 1c and 1d, respectively.

2.1. Coupled H1D-K2 model

The KINEmatic runoff and EROSion model (KINEROS2, K2) is a widely used and open-source watershed model representing a watershed by a cascade of overland flow planes and channels (Smith et al., 1999, Goodrich et al., 2012). The overland flow is described using the kinematic wave approximation of the Saint-Venant equations (assuming uniform flow and a friction slope approximately equal to the plane slope) (Woolhiser et al., 1970, Giráldez and Woolhiser, 1996). The kinematic wave solution is accurate for most overland flow conditions (Woolhiser and Liggett, 1967, Goodrich et al., 2012). The kinematic wave equation can be expressed as follows:

$$\frac{\partial h}{\partial t}+\frac{\partial Q}{\partial x}=q(x,t) \tag{1}$$

where h is the surface water depth [m], t is time [s], x is the distance coordinate over the plane [m], Q is the discharge per unit width [m^2/s], and $q(x,t)$ is the change of the lateral inflow rate [m/s], which is equal to local precipitation rate minus local infiltration and evapotranspiration rates.

Discharge per unit width (Q) is related to the surface water depth (h) by a simple power relation (Giráldez and Woolhiser, 1996):

$$Q=\alpha h^{m} \tag{2}$$

where parameters α [$m^{1/3}s^{-1}$] and m [-] are related to the slope, surface roughness, and flow conditions (laminar or turbulent flow). The Manning hydraulic resistance law is commonly used to obtain the

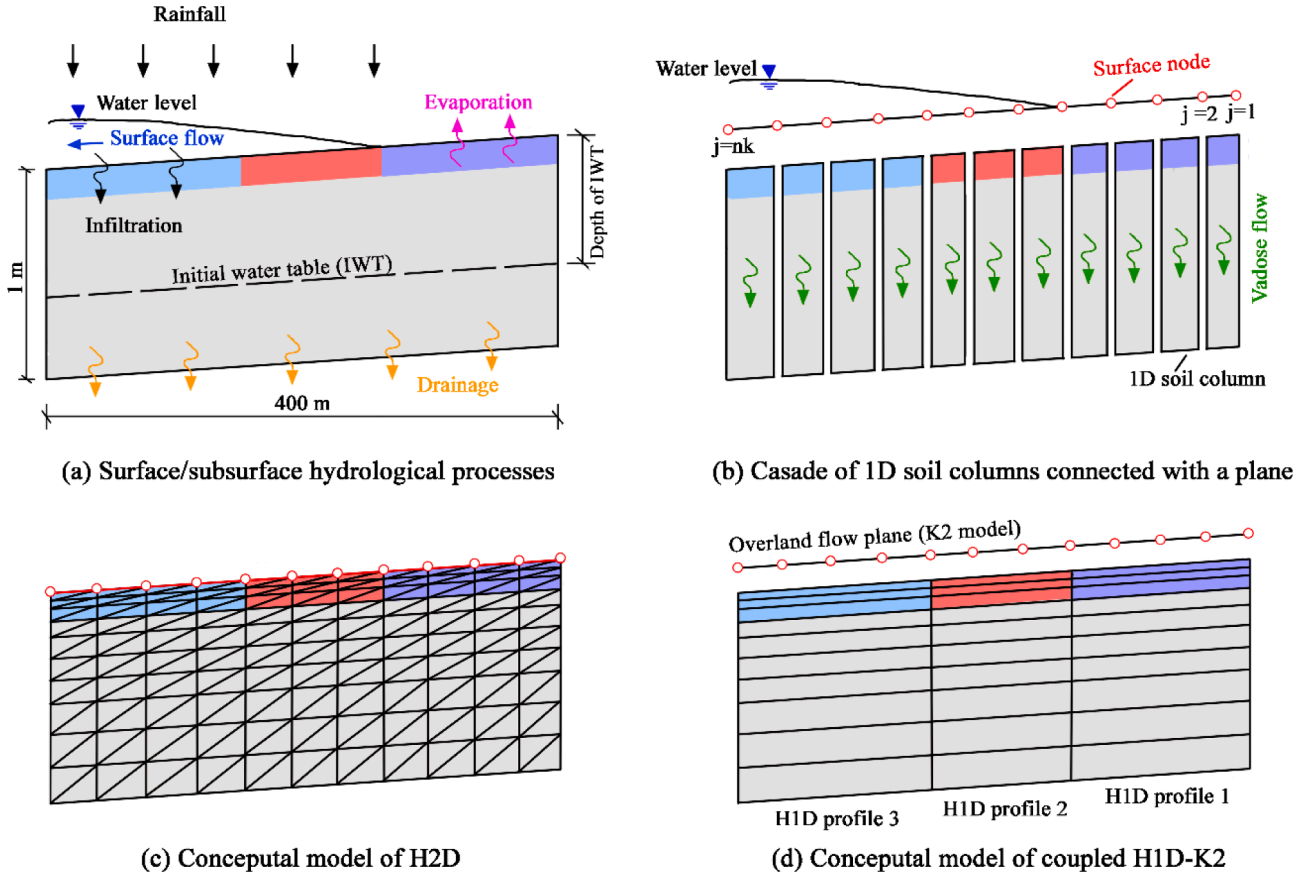

Fig. 1. (a) The conceptual model of surface/subsurface hydrological processes; (b) a cascade of 1D soil columns connected with an overland flow plane, where each soil column is linked to one surface node ($j = 1, 2, \ldots, nk$); (c) a conceptual model of a hillslope simulated by the H2D model; and (d) a conceptual model of a hillslope simulated by the coupled H1D-K2 model, where one or multiple H1D columns are linked to multiple surface nodes (one vertical soil column for a homogeneous system and three columns for a heterogeneous system in this study). Note: the red circle represents the discretization nodes for solving the surface flow equation. The red and yellow lines represent the applied boundary conditions (BCs) at the land surface and the bottom of a soil profile, respectively. No flow BCs were applied on the vertical sides of the 2D model. Different color zones represent different soil types at the soil surface (0 ~ 0.05 m), while the subsurface is uniform. K_{s1}, K_{s2}, and K_{s3} are the near-surface hydraulic conductivities of the uphill (purple zone), middle (red zone), and downhill (blue zone) sections, respectively. (For interpretation of the references to color in this figure legend, the reader is referred to the web version of this article.)

parameter α:

$$\alpha = \frac{k}{n} S^{1/2} and m = \frac{5}{3} \quad (3)$$

where S is the slope [–], and n is a Manning's roughness coefficient for overland flow [$m^{1/3}s^{-1}$], k is a unit conversion factor between International System (SI) and English units. $k = 1$ ($m^{1/3}\ s^{-1}$) for SI units and 1.49 ($ft^{1/3}\ s^{-1}$) for English units.

The K2 model has been applied to investigate the processes of interception, infiltration, runoff generation, erosion, and sediment transport (up to five particle sizes) for individual rainfall-runoff events (Giráldez and Woolhiser, 1996, Goodrich et al., 2006, Guber et al., 2014, Meles Bitew et al., 2020). Infiltration is described using an equation for cumulative vertical infiltration into a homogeneous (infinite) soil profile with uniform initial moisture content (Parlange et al., 1982). The K2 model can also consider a two-layer soil profile without a bottom boundary condition to represent differences in soil texture in the subsurface. K2 cannot simulate saturation excess overland flow (Fig. S5) because it assumes an infinitely deep soil profile. Furthermore, the K2 model does not provide information on the spatial and temporal variability of water content and neglects evaporation. These limitations restrict the ability of the K2 model to investigate surface–subsurface connectivity.

To overcome the above-discussed limitations, we have developed a novel coupling approach to replace the empirical infiltration equation in the K2 model with the physically-based H1D model. H1D simulates 1D variably saturated water flow in the vadose zone by numerically solving the Richards equation (Fig. 1d) and using realistic BCs at the soil profile bottom (Simunek et al., 2005). Evapotranspiration processes are accounted in H1D but are not considered in this paper since their impact on the runoff generation is relatively small for the considered time scales. The total simulation time is divided into multiple periods (Δt_p), which are usually larger than the individual time steps (Δt_i) for solving the surface and subsurface equations. Furthermore, convergence conditions are employed to automatically adjust time steps in both the H1D (Simunek et al., 2005) and K2 (Goodrich et al., 2012) models. To improve computational efficiency, one soil profile is used to represent the entire subsurface domain when soil characteristics do not vary horizontally but may change in the vertical direction. When soil properties vary horizontally, the overland flow plane is divided into multiple sections, each connecting to one soil type (Fig. 1d).

A MATLAB script executes the H1D and K2 codes sequentially. A series of MATLAB functions read and write the input and output files, initialize local and global variables, and update exchange information at a selected Δt_p. Fig. 2 shows a flowchart depicting the coupling approach in the H1D-K2 model. This coupling sequence is summarized below:

(1) The H1D code is executed with the applied land surface BCs (i.e., rainfall, evaporation) to obtain the actual infiltration and evaporation rates. The land surface BC of each H1D soil profile is determined using the surface water depth calculated in the previous Δt_p. If there is no ponding, an atmospheric BC is used. When water starts ponding at the soil surface, the land surface BC is switched from an atmospheric BC to a constant pressure head BC. The corresponding pressure head value is equal to the average water depth of surface nodes in an overland flow plane. If multiple H1D soil profiles are set, a loop is employed to estimate infiltration for each soil profile (Fig. 2).

(2) A water balance considering infiltration, rainfall, evaporation, and ponded water is performed to determine if the soil infiltration capacity (q_{soil}) exceeds the water supply (q_{supply}, the sum of rainfall, inflow from a neighboring plane, and ponded water minus evaporation). When the pressure head BC is imposed, the infiltration volume over a Δt_p is

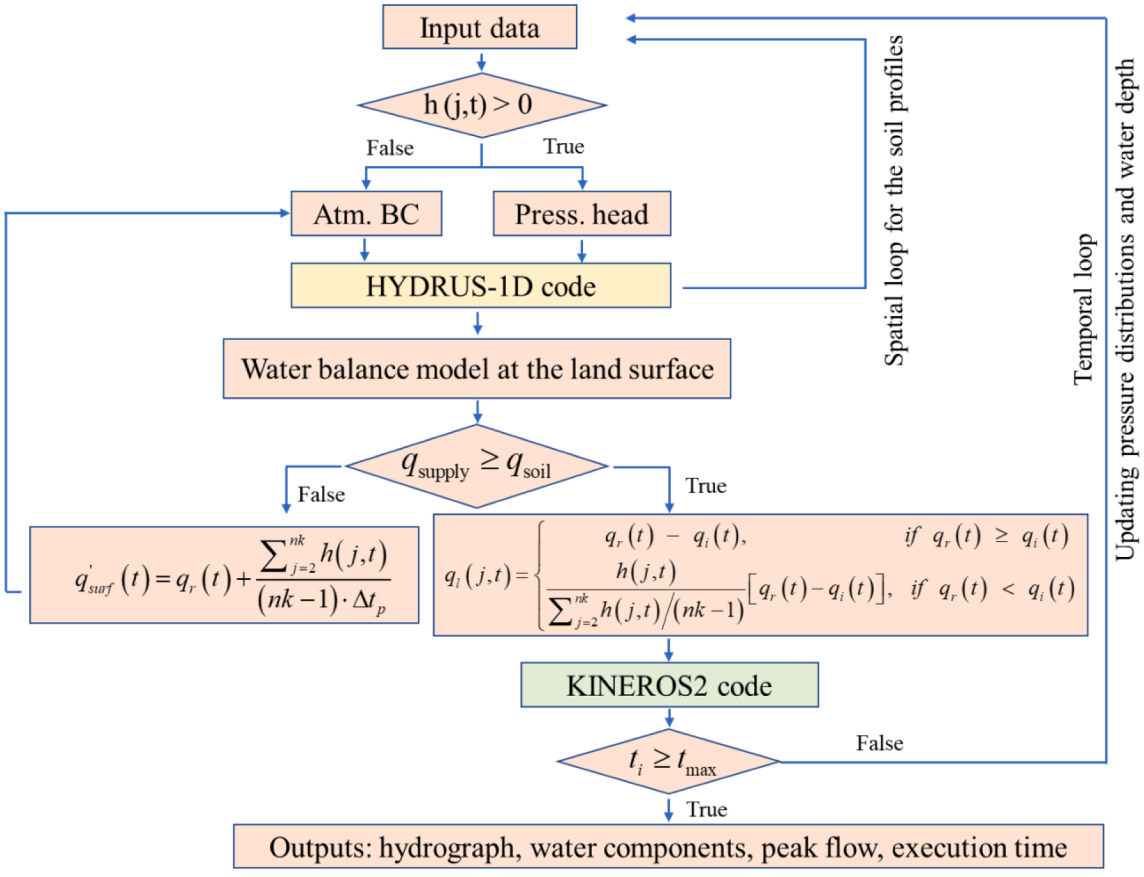

Fig. 2. Flowchart depicting the data flow in the coupled H1D-K2 code. Orange color indicates computations in MATLAB. (For interpretation of the references to color in this figure legend, the reader is referred to the web version of this article.)

controlled by q_{soil} rather than by water supply, and calculated cumulative infiltration may be larger than q_{supply}. The pressure head BC will overestimate infiltration when the soil infiltration capacity exceeds the water supply. The pressure head BC for the subsurface equation is therefore switched to an atmospheric BC if this exceedance occurs. The H1D code will maintain water balance when using an atmospheric BC that considers the actual infiltration rate and the maximum water supply volume during Δt_p. The potential surface flux (q'_{surf}) is set equal to rainfall rate (q_r) plus the ponding water contribution given as:

$$q'surf(t) = q_r(t) + \frac{\sum_{j=2}^{nk} h(j,t)}{(nk-1)\Delta t_p} \tag{4}$$

where $h(j,t)$ is the time-series of surface water depths at the surface node, and j is the surface node number starting from node 1 and ending with node nk. Note that the second term on the right side of Eq. (4) gives the mean surface water depth for all surface nodes ($j = 1, 2, \ldots, nk$) divided by the Δt_p. The subsurface equation is then solved with the surface water depths at the previous time as an initial condition and the new specified flux BC. The criterion used to stop each iteration cycle is the difference between cumulative infiltration and cumulative water supply over the time interval being less than 10^{-6} m^2.

(3) The time-series of net surface flux $q_l(j,t)$ (i.e., the difference between rainfall, evaporation, and actual infiltration) generated by the H1D is then applied to the corresponding surface nodes in the K2 code. When rainfall is larger than actual infiltration, positive q_l is redistributed at the land surface and routed down over the overland flow plane. In the case of negative q_l, ponded water infiltrates into the subsurface, and its absolute value is subtracted from the surface storage of each surface node while solving the surface water routing equation. Note that $q_l(j,t)$ in an H1D profile corresponds to vertical inflow from multiple surface nodes in the K2 calculation (Fig. 1d). Therefore, a new method is used to assign the time series of $q_l(j,t)$ in the overland plane. A weighting factor is calculated as a ratio of the surface water depth at each surface node and the average surface water depth of an entire plane at the end of the previous Δt_p. It is reasonable to assume that cumulative infiltration into the soil with a higher ponding depth is larger than the one with a smaller ponding depth. When the surface water depth at a surface node is zero, $q_l(j,t)$ is zero as well. Additionally, the K2 code was modified to save and initialize local and global variables with the previously calculated results so that $q_l(j,t)$ is applied to the corresponding surface nodes. The net surface flux is obtained by:

$$q_l(j,t) = \begin{cases} q_r(t) - q_i(t) if q_r(t) \geqslant q_i(t) \\ \dfrac{h(j,t)}{\sum_{j=2}^{nk} h(j,t)/(nk-1)} [q_r(t) - q_i(t)] if q_r(t) < q_i(t) \end{cases} \tag{5}$$

where q_i is the infiltration rate.

(4) The K2 code is executed to calculate lateral water flow on the land surface while considering the feedback of the subsurface hydrological processes. Surface water depths at each surface node and the outflow rate from the overland plane are simulated during Δt_p.

(5) Calculated pressure heads are set as the initial condition for the H1D computation at the next Δt_p. The information on water depths is updated for the K2. After that, a temporal loop is executed until the total simulation time (t_i) reaches the final time (t_{max}).

2.2. HYDRUS-2D (H2D) model with an overland flow routine

The H2D (version 3) model with an overland flow routine was used to simulate runoff at the land surface and water infiltration and redistribution processes in the vadose zone (Šimunek, 2003, Simunek, 2015). Water flow in the vadose zone is described using the Richards equation, while the overland flow is described using the kinematic wave equation (Eq. (1)). The water exchange rate between the surface and subsurface domain is represented using the source term in the surface flow equation (Eq. (1)), while the applied land surface BCs account for the effects of surface water conditions on subsurface flow. The soil-hydraulic functions of van Genuchten (1980) are used to obtain unsaturated soil hydraulic properties.

The atmospheric BC with surface runoff is applied on the land surface to reflect the surface conditions, and BC switching between the variable pressure head and the atmospheric-controlled conditions (i.e., precipitation and evaporation) are implemented to represent ponding or no ponding conditions, respectively. At any given time step, the subsurface equation is solved first for prescribed initial conditions and an atmospheric BC. After that, a water balance calculation is performed to calculate the exchange flux and distribute it to separate surface and subsurface nodes. Once surface ponding is reached at any surface node (once q_{soil} is smaller than $q_l(j,t)$), overland flow is generated. The surface water is routed to the lower parts of the hillslope via a kinematic wave equation. When water is ponded at the soil surface, the land surface BC is switched to a variable pressure head BC. Surface water depths at each surface node are updated at each time step. The output information is printed for each node where the overland flow becomes active. Details concerning the theory, numerical solution techniques, and example applications of H2D are given by Šimunek and van Genuchten (2008) and Kohne et al. (2011).

3. Benchmark cases

The hydrological processes on a hillslope with a length (L) of 400 m and subsurface thickness of 1 m (Fig. 1a) were simulated and compared using the H2D and coupled H1D-K2 models. The subsurface was discretized into 100 finite elements with the mesh size varying from 0.0053 m near the soil surface to 0.012 m at the soil bottom. The horizontal mesh size was 2 m for the H2D model and 10 m for the K2 model. The total number of surface nodes was 41 in the K2 model. The first surface node was used to receive inflow from uphill (not considered in this study). Finer horizontal discretization was used in the H2D model because coarse (>2 m) spatial discretization causes numerical oscillation problems for the heterogenous hillslope with a steep slope. The subsurface spatial heterogeneity in the horizontal direction determines the number of H1D profiles. At least three H1D soil profiles were needed to reflect the spatial heterogeneity in Fig. 3b and 3c. For the model with three soil profiles, the uphill, middle, and downhill H1D soil profiles correspond to 15, 10, and 15 surface nodes, respectively. For the coupled H1D-K2 model with 40 soil profiles, each surface node relates to one H1D soil profile. Furthermore, an analytical solution of overland flow on an impermeable plane served as a base case to evaluate the model performance. The subsurface with the saturated hydraulic conductivity of 10^{-11} m/min was assumed to be impermeable, and modeled results were compared with the analytical solution.

The performance of the coupled H1D-K2 code was tested against H2D for homogeneous and heterogeneous conditions with horizontally different saturated hydraulic conductivities (K_s), initial water content distributions, bottom BCs (i.e., no flow and free drainage), slope ratios, and rainfall intensities and durations. Detailed model setups are listed in Table 1. Four slopes (0.0005, 0.001, 0.0025, and 0.01) were selected to test the impact of the surface flow speed on infiltration and overland flow, while two bottom BC types were employed to test the feedback between the subsurface and surface flow processes. The bottom BC is used to represent the exchange flux between the vadose zone and groundwater. The no-flow BC represents an impermeable bottom layer, while the free drainage BC allows for water to drain from the bottom of the soil profile by gravity (Simunek et al., 2005).

Time step and iteration criteria settings in the H1D and H2D models were the same to obtain comparable results. The pressure head and water content tolerances were equal to 0.01 m and 0.001, respectively. The initial pressure head distribution was assumed to be hydrostatic equilibrium with a given top pressure head. The same initial pressure

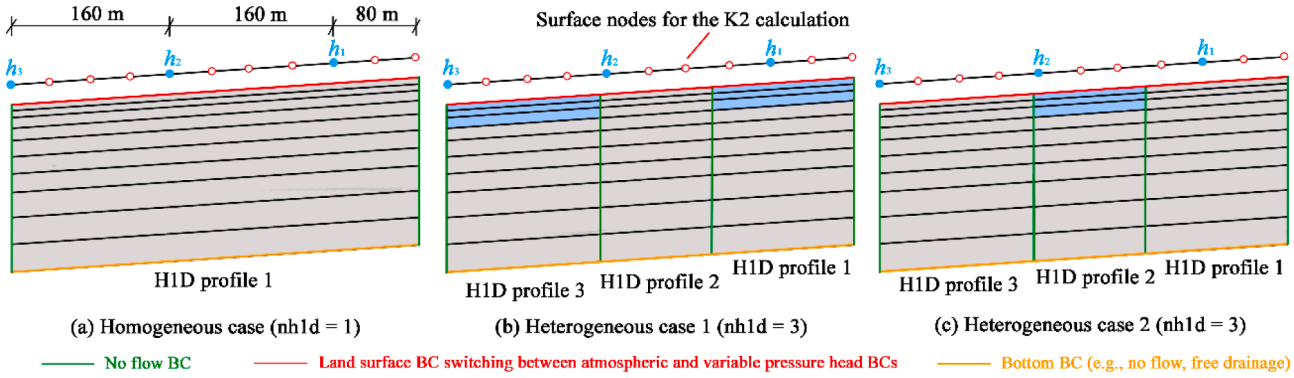

Fig. 3. The conceptual model simulated by the coupled H1D-K2 model for (a) a homogeneous case, (b) heterogeneous case 1, and (c) heterogeneous case 2. The subsurface of an overland plane is uniform, except for the blue zones with a K_s of 6.94 × 10^{-6} m/min. The blue points h_1, h_2, and h_3 are observation nodes. nh1d is the number of the H1D soil profiles. (For interpretation of the references to color in this figure legend, the reader is referred to the web version of this article.)

Table 1
Mesh size, initial and boundary conditions, and parameters for the benchmark cases.

	Homogeneous subsurface				Heterogeneous subsurface	
	Base case	Excess saturation	Excess infiltration	Multiple rainstorms	Case 1	Case 2
Mesh size						
HYDRUS-2D						
Horizontal mesh size, Δx (m)	2.0	2.0	2.0	2.0	2.0	2.0
Coupled H1D-K2 model						
Horizontal mesh size, Δx (m)	10.0	10.0	10.0	10.0	10.0	10.0
Exchange period, Δt_p (min)	10, 100*	10, 100*	10, 100*	2**, 10	10	10
Number of H1D soil profiles	1	1	1	1	3	3
Initial and boundary conditions						
Depth of initial water table, *IWT* (m)	0.0	0.5, 0.75, 1.0	1.0	1.0	1.0	1.0
Rainfall rate, q_r ($\times 10^{-4}$ m/min)	3.3	3.3	3.3	0.33, 3.3	3.3	3.3
Bottom BCs	no flow	no flow	no flow	no flow, free drainage	free drainage	no flow
Slope, (-)	0.0005	0.0005	0.0005	0.0005	0.01	0.0005
Manning's roughness coefficient, ($\times 10^{-4}$)	3.31	3.31	3.31	3.31	3.31	3.31
Saturated hydraulic conductivity, K_s ($\times 10^{-5}$m/min)	10^{-6}	69.4	69.4, 6.94, 0.694	6.94	0.694, 69.4	0.694, 69.4
van Genuchten parameters						
θ_{sat} (-)	0.4	0.4	0.4	0.4	0.4	0.4
θ_{res} (-)	0.08	0.08	0.08	0.08	0.08	0.08
n_0 (-)	2.0	2.0	2.0	2.0	2.0	2.0
α_0 (1/m)	1.0	1.0	1.0	1.0	1.0	1.0

Notes: Symbol "*" indicates that the exchange period of 100 mins was used to simulate a hillslope with a no-flow BC. Symbol "**" indicates that the exchange period of 2 mins was used to simulate a hillslope with a no-flow BC and a slope of 0.01. The initial water table depth (IWT) is defined as the water table depth relative to the ground surface at the beginning of the calculation. θ_{sat} and θ_{res} are the saturated and residual water contents, respectively. α_0 is a parameter corresponding approximately to the inverse of the air-entry value, cm^{-1}, and n_0 is an empirical shape-defining parameter.

head distribution was used for both the H1D and H2D models. Both initial and minimum time steps were set at 10^{-6} min, and the maximum time step was set to 1 min. The maximum number of iterations was equal to 10. All simulations were carried out for 300 mins, except for cases with multiple rainstorms (1200 mins). The rainfall rate was applied for 200 mins, followed by 100 mins of recession ($q_r = 0$). For the coupled H1D-K2 model, the duration of water exchange (Δt_p) between surface and subsurface varied from 2 to 100 mins, depending on the slope and heterogeneity of the overland plane. Simulation outputs were reported at a one-min interval. The van Genuchten parameters are listed in Table 1.

The performance of the coupled H1D-K2 code was evaluated by comparing its results with the output of the H2D model, including the time-series of outflow rates, surface water depths at three observation points (h_1, h_2, and h_3, shown in Fig. 3), and the surface water storage. Furthermore, the relative mass balance error (MBE) evaluated the errors caused by the coupling strategy and numerical methods used in the two domains. The relative MBE was computed for the entire hillslope domain using the following equation:

$$RelativeMBE = \left| \frac{\int_0^{t_{max}} [q_r(t) - q_e(t) - q_d(t)]dt \cdot L - \int_0^{t_{max}} q_{out}(t)dt - \Delta q_{surf} - \Delta q_{sub}}{\int_0^{t_{max}} q_r(t)dt} \right| \quad (6)$$

where Δq_{surf} (m^2) and Δq_{sub} (m^2) are the changes in the surface and subsurface storages over the total simulation time, respectively, q_e is the evaporation rate (m/min), q_d is the drainage at the soil profile bottom (m/min), and q_{out} is the outflow rate (m^2/min).

The ability of the coupled H1D-K2 model to predict spatial and temporal water content distributions depends on the number of vertical soil profiles employed. We, therefore, simulated and compared three models: H2D (served as a reference), the coupled H1D-K2 model with one (for a homogeneous case) or three (for a heterogeneous case) soil profiles, and the coupled H1D-K2 model with 40 soil profiles. Kriging interpolation with a linear semi-variogram model was used to estimate the water content distribution. Water content variations with depth and time were also compared to evaluate vadose zone flow (Figs. S1 and S2). To illustrate the accuracy and robustness of the proposed H1D-K2 model over a wide range of conditions, we simulated and compared outflow

rates and cumulative runoffs for 32 cases with those obtained by the H2D model. The detailed descriptions of the sensitivity analysis, the related results, and the discussion are given in the Supporting Material (Fig. S3). In general, simulation results show that the coupled H1D-K2 model can accurately and efficiently simulate the surface and subsurface hydrological processes on a hillslope under scenarios with different spatial heterogeneities (Fig. 3), slopes (i.e., 0.0005, 0.001, 0.0025, and 0.01), and bottom BCs (i.e., no flow and free drainage). The overland flow plane connecting one (homogeneous cases) and three (heterogeneous cases) H1D profiles with different soil layering can capture the general hydrological behavior at the surface and in the subsurface (Fig. S3), which is similar to the results of integrated hydrologic models used in previous studies (e.g., Simunek 2003, Sulis et al., 2010, Kollet et al., 2017, Coon et al., 2020). Under a uniform rainfall storm, the runoff pattern was sensitive to the spatial heterogeneity, while its magnitude was related to the drainage condition at the bottom (Fig. S3).

3.1. Runoff generation on a homogeneous hillslope with uniform rainfall

Two homogeneous and isotropic planes with impervious and pervious soils and a slope of 0.0005 were used to evaluate the model performance in predicting surface runoff in response to uniform rainfall. For the coupled H1D-K2 model, one soil profile was used to simulate water flow in the subsurface (Table 1). The rainfall rate ($q_r = 3.3 \times 10^{-4}$ m/min) was applied for the first 200 mins, followed by 100 mins of recession ($q_r = 0$ m/min). The total simulation time was 300 mins (Table 1).

An analytical solution of the kinematic wave equation on an impervious rectangular plane (Gottardi and Venutelli, 1993) was used to compare simulated outflow rates using the coupled H1D-K2 and H2D models. The parameters used in the analytical solution (base case) are listed in Table 1. The detailed information, including the mathematical equation, parameters, and BCs can be found in Gottardi and Venutelli (1993) and Jaber and Mohtar (2003).

The mechanism for runoff generation is mainly classified into two types: saturation excess (Dunne) runoff and infiltration excess (Horton) runoff (Smith and Woolhiser, 1971, Fatichi et al., 2016). For the Dunne runoff, surface ponding occurs after the soil saturates and water fills the subsurface storage. To realize this runoff generation mechanism, the saturated hydraulic conductivity ($K_s = 6.94 \times 10^{-4}$ m/min) was specified to be larger than the rainfall rate ($q_r = 3.3 \times 10^{-4}$ m/min). Three simulations with different depths of the initial water table (IWT) were tested (Table 1). Conversely, for the Hortonian overland flow, the surface ponding occurs when the rainfall rate exceeds the infiltration rate ($K_s < q_r$). Three simulations with the same IWT depth of 1 m and different K_s (6.94×10^{-5} m/min, 6.94×10^{-6} m/min, and 6.94×10^{-11} m/min) were considered.

3.2. Runoff generation on a heterogenous hillslope

A hillslope transect with two soil materials was simulated to consider spatial heterogeneity of subsurface hydraulic properties on the runoff generation. To demonstrate the robustness of the coupled H1D-K2 model, we considered two heterogeneous cases in which high or low permeability zones are near the surface (0–0.05 m) compared to the rest of the soil materials. Heterogeneous case 1, similar to a test problem introduced in Šimunek (2003), uses a high permeable near-surface (0.05 m) middle section (Fig. 1d and 3) with a K_s value of (6.94×10^{-4} m/min) that is two orders of magnitude higher than the rest of the uniform subsurface with a K_s of 6.94×10^{-6} m/min. Heterogeneous case 2 is similar to Kollet and Maxwell (2006) with a low permeable near-surface (0.05 m) soil in the middle of the hillslope, and a K_s value two orders of magnitude smaller (6.94×10^{-6} m/min) than the remaining soil ($K_s = 6.94 \times 10^{-4}$ m/min). Both heterogeneous cases employed three H1D soil profiles to describe subsurface water flow in the hillslope's uphill, middle, and downhill sections (see Fig. 1b and S1).

The length of the middle section was 100 m, while it was 150 m for both uphill and downhill sections. A rainfall rate ($q_r = 3.3 \times 10^{-4}$ m/min) was applied for the first 200 mins, followed by the 200 mins of recession ($q_r = 0$ m/min). The slopes were 0.01 and 0.0005 for case 1 and case 2, respectively. Free drainage and no flow BCs were applied at the bottom of the soil profiles in case 1 and case 2, respectively. These two benchmark cases have been used in the intercomparison of integrated hydrologic models (e.g., Sulis et al., 2010, Simunek 2015, Kollet et al., 2017, Coon et al., 2020).

3.3. Runoff generation on a homogeneous hillslope with multiple rainstorms

Four different configurations (slopes of 0.0005 and 0.01, and no flow and free drainage bottom BCs) with multiple rainstorms were considered to examine the stability of the coupled H1D-K2 model. The rainfall rate ($q_r = 3.3 \times 10^{-4}$ m/min) was applied for the first 200 mins, then decreased to 1.0×10^{-4} m/min for the next 200 mins, followed by 200 mins of recession ($q_r = 0$ m/min). The rainfall events were repeated in the next 600 mins. The total simulation time was 1200 mins. The soil was assumed to be homogeneous and isotropic with a K_s of 6.94×10^{-5} m/min. The H1D-K2 model only employed one soil profile to represent vadose zone flow in these simulations (Table 1).

4. Results

4.1. Surface runoff over a homogeneous subsurface with a uniform rainfall rate

Simulation results for the H2D and coupled H1D-K2 models have excellent agreement with the analytical solution for the low-permeability subsurface (6.94×10^{-11} m/min) (Fig. 4a) and saturated condition (Fig. 4b). The average errors were less than 0.5 % in both cases. Simulated outflow rates for the H2D and H1D-K2 models were in good agreement for both infiltration excess (Fig. 4a) and saturation excess (Fig. 4b) conditions. Differences were less than 0.9 % in outflow rates and less than 0.5 % in the cumulative outflow.

4.2. Surface runoff over a heterogeneous hillslope with a uniform rainfall rate

4.2.1. Heterogeneous case 1

The hydrograph simulated by the H2D model (Fig. 5a) shows that outflow began at 3.8 mins, experienced a steep increase to 6.52×10^{-4} m^2/s, remained constant until the arrival of the second wave at 145 mins, and then gradually increased and reached peak flow (6.99×10^{-4} m^2/s). After rainfall stopped ($t = 200$ mins), the outflow rate decreased gradually to zero at 229 mins. Similar outflow rates were obtained for case 1 by the coupled H1D-K2 model when a high-permeability zone was placed near the surface in the middle section of the hillslope. The onset and cessation of surface runoff were almost identical for the three hydrological models.

Simulated surface water depths at observation points h_1 and h_3 were almost identical for all three models (Fig. 5b). The biggest difference occurred in predicting the onset of water ponding at h_2 node located on the high permeability section of the hillslope. The corresponding values for the H2D model, the coupled H1D-K2 model with 40 soil profiles, and the coupled H1D-K2 model with three soil profiles were 92 mins, 82 mins, and 122 mins, respectively. The maximum differences in the surface water depth were less than 0.2 mm among the three models.

Table 2 shows that differences in simulated water balance components of heterogeneous case 1 were very small among the three models. Compared to the results produced by H2D, peak flow predicted by the coupled H1D-K2 model with 40 and three soil profiles was approximately 8.0 % higher, while the cumulative outflow was quite similar (2.2–3.4 % difference). The shortest computation time was for the

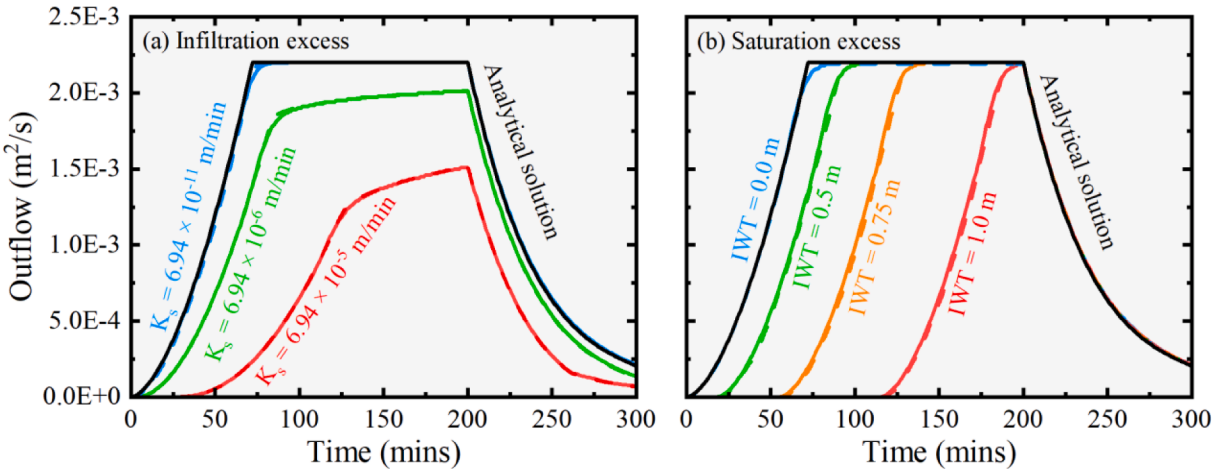

Fig. 4. Outflow rates for (a) infiltration excess and (b) saturation excess, simulated by the H2D (dashed color lines) and coupled H1D-K2 codes (solid color lines). The hillslope is homogeneous, with a no-flow BC applied at the bottom. Note: IWT represents the initial water table. The solid black lines represent the base case (analytical solution).

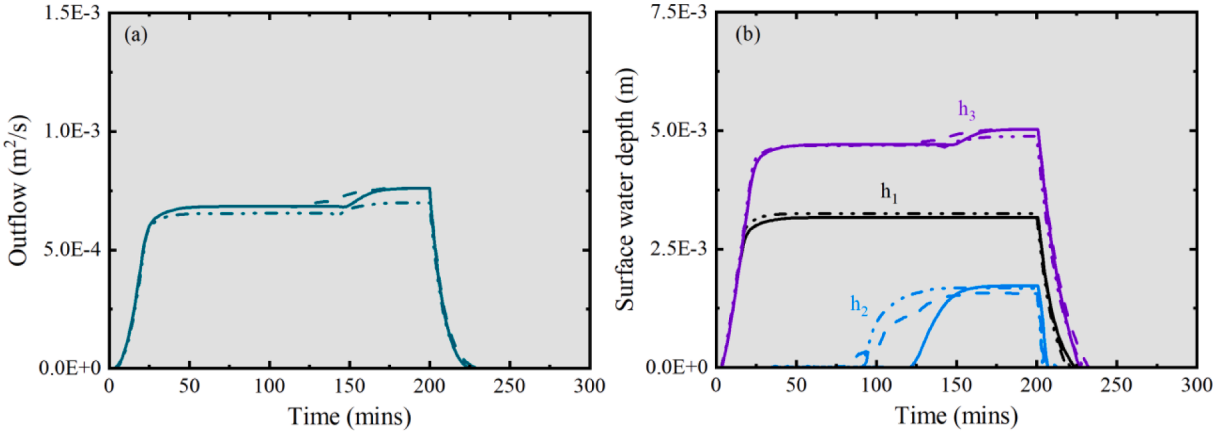

Fig. 5. (a) Outflow rates for heterogeneous case 1 with a slope of 0.01 and the free drainage BC applied at the bottom; and (b) surface water depth at the observation points of h_1, h_2, and h_3, simulated by the H2D (dash-dotted lines) and coupled H1D-K2 codes with three soil profiles (solid lines) and 40 soil profiles (dashed lines).

Table 2
Mass balance components for heterogeneous case 1 with a slope of 0.01 and the free drainage BC applied at the bottom.

	Cum. precip. (m^2)	Cum. outflow (m^2)	Cum. drain. (m^2)	Surface storage (m^2)	Subsurface storage (m^2)	Relative MBE (%)	Onset of outflow (mins)	Peak flow (m^2/s)	Comp. time (s)
H2D	26.40	7.57	28.90	0.00	−10.04	0.01	3.8	6.99×10^{-4}	32.49
H1D-K2 (nh1d* = 40)	26.40	8.07	30.49	0.00	−11.97	0.72	3.0	7.60×10^{-4}	321.74
H1D-K2 (nh1d* = 3)	26.40	7.97	29.58	0.00	−11.09	0.22	3.0	7.60×10^{-4}	21.36

Note: *nh1d – the number of the H1D soil profiles.

coupled H1D-K2 model with three soil profiles (21.36 s), followed by the H2D model (32.49 s), while the coupled H1D-K2 model with 40 soil profiles had the longest computation time (321.74 s).

Fig. 6 demonstrates similar subsurface water content distributions simulated by the three models in response to the rainfall-runoff processes in case 1. Since the rainfall intensity exceeds the infiltration capacity of the lower and upper sections of the hillslope, water ponding occurs quickly in these two sections and is routed downslope, either off the hillslope or to the midsection (Fig. 6a). As rainfall intensity does not exceed the infiltration capacity of the midsection, no ponding due to rainfall occurs. Instead, the ponded water from the upper part of the hillslope was routed downslope and infiltrated into the subsurface in the midsection causing earlier arrival of the saturation front in the middle section of the hillslope with higher permeability. After the cessation of the rainfall, water drained out from the bottom of the soil profile, causing a decrease in the water content. The H2D model and the coupled H1D-K2 model with 40 soil profiles very well reproduced the overland and subsurface water movement behavior. Conversely, as expected, only the horizontally averaged saturation front characteristics were captured in the middle section by the coupled H1D-K2 model with three soil

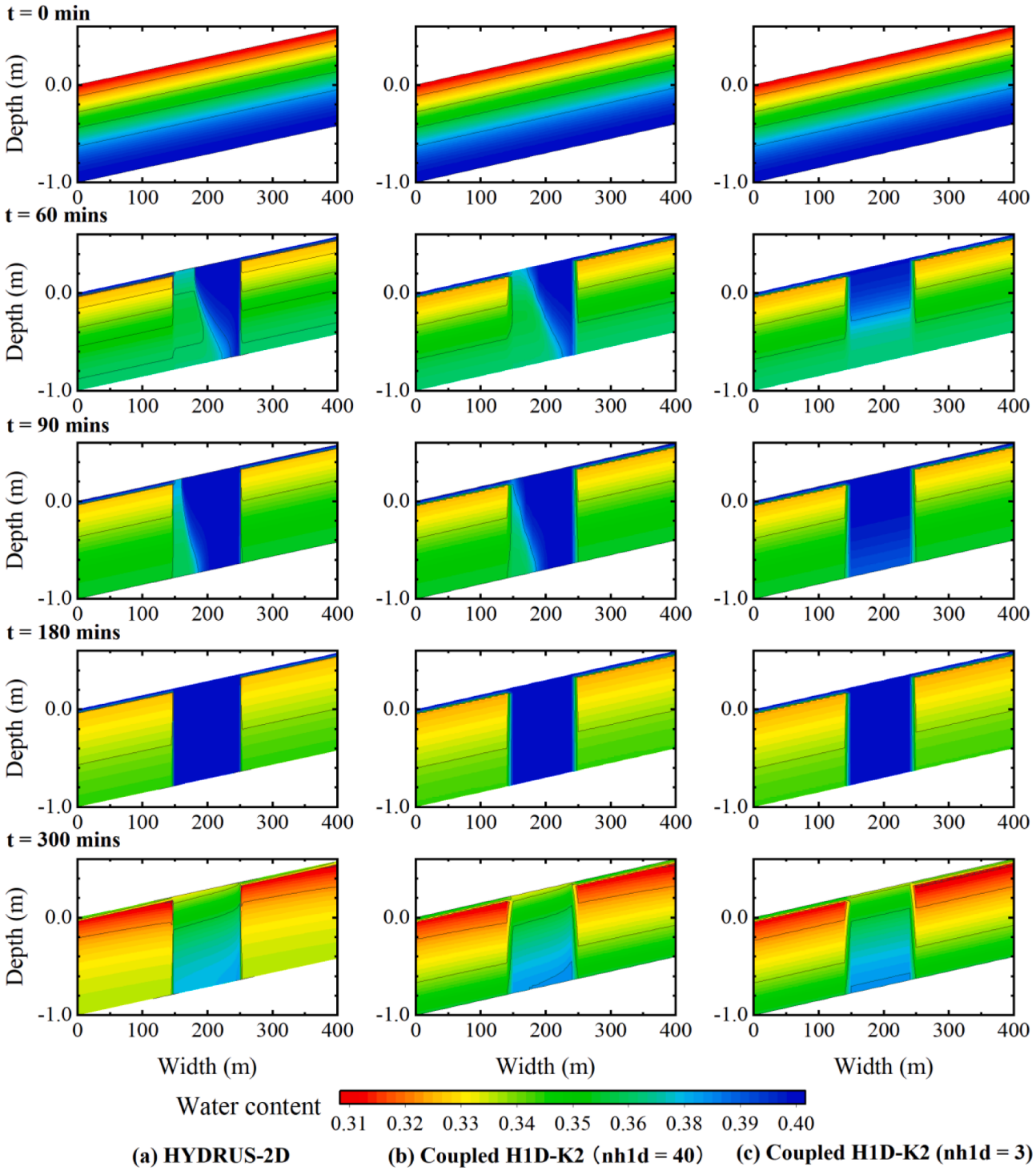

Fig. 6. Simulated water content distributions for heterogeneous case 1 with a free drainage BC at the bottom of the soil profile below the overland flow plane with a slope of 0.01 at times of 0, 60, 90, 110, and 300 mins (top to bottom) simulated by H2D (left), coupled H1D-K2 with 40 soil profiles (middle), and coupled H1D-K2 with three soil profiles (right). The vertical distance is not at scale. nh1d is the number of the H1D soil profiles.

profiles, where this section was represented by only one soil profile. Although this model significantly simplifies the real conditions, it could produce the overall hydrological behavior of this entire system (e.g., outflow rate and peak, average subsurface saturation) sufficiently well for most practical problems.

4.2.2. Heterogeneous case 2

Fig. 7a shows the hydrograph simulated by the three models for heterogeneous case 2 (low-permeability zone located in the middle of the hillslope). H2D predicts that the outflow occurs at 108.3 mins, experiences a step increase to 1.25×10^{-3} m^2/s after several mins, then remains constant for about 50 mins before gradually reaching the peak flow (2.08×10^{-3} m^2/s) and a slow recession once rainfall stops (at 200 mins). After cessation of the rainfall (t = 200 mins), the outflow rate decreased gradually, dropping to 1.59×10^{-4} m^2/s at the end of the simulation. The coupled H1D-K2 model shows very similar outflow behavior as the H2D model, with the only difference in the early onset of predicted surface runoff of 4 and 17 mins for the H1D-K2 models with 40

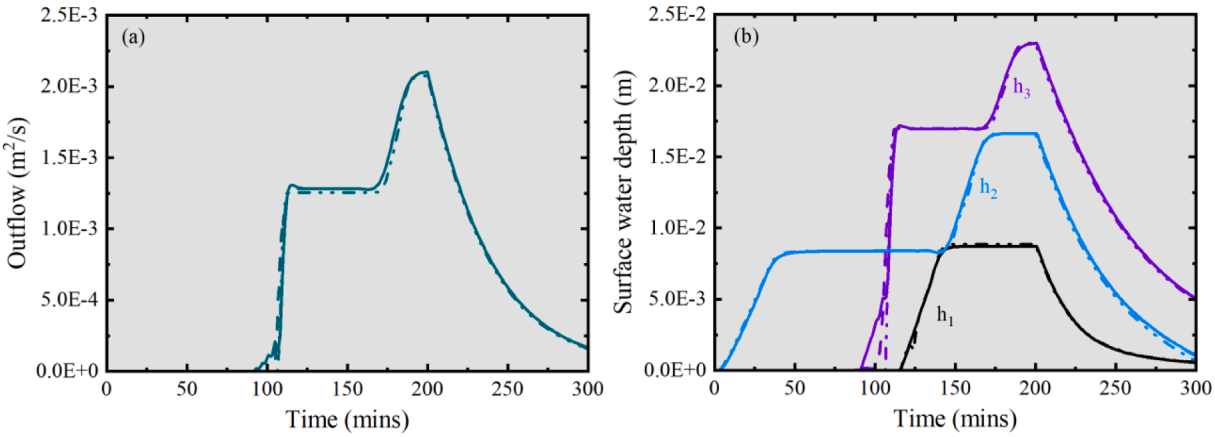

Fig. 7. (a) Time-series of the outflow rate and (b) variations of surface water depths at observed points h_1, h_2, and h_3 for a heterogeneous hillslope (case 2) with a slope of 0.0005 and a no-flow BC applied at the bottom, simulated by the H2D (dash-dotted lines), and coupled H1D-K2 code with three soil profiles (solid lines) and 40 soil profiles (dashed lines).

and three soil profiles, respectively. All three models predicted the same trend of surface water depths at points h_1 and h_2 (Fig. 7b), with the only minor differences in the onset of runoff at point h_3 (Fig. 6b).

Fig. 8a shows the water content distributions simulated by H2D at selected times. Ponded water from the low-permeability zone (the middle section of the hillslope) was routed toward the outlet and infiltrated into the downhill portion of the hillslope. The saturation front gradually moved downward and toward the outlet. Because of the additional water source from the midsection, full surface saturation was achieved faster in the downhill section than in the uphill portion of the hillslope. Similar water content distributions were observed for the H2D model and the H1D-K2 model with 40 soil profiles (Fig. 7a and 7b). Conversely, the coupled H1D-K2 model with three soil profiles could not fully capture the same water content distribution dynamics. In particular, the routed surface water infiltrated and redistributed in the vertical direction and reached saturation after 90 mins in the downhill portion of the hillslope.

Table 3 summarizes components of the simulated water balance for the three models for heterogeneous case 2. Differences in cumulative outflow and peak flow were less than 0.3 % for the coupled H1D-K2 model with 40 and three soil profiles compared to H2D. The simulated peak flow and time were the same for all three models. Moreover, the coupled H1D-K2 model with three soil profiles had the shortest computation time (16.71 s), followed by the H2D model (24.35 s). The coupled H1D-K2 model with 40 soil profiles had the longest computation time (145.92 s).

4.3. *Surface runoff over a homogeneous subsurface with multiple rainstorms*

4.3.1. *No flow bottom BC*

Fig. 9a shows hydrographs simulated by the H2D and H1D-K2 (with a single soil profile) models in response to multiple rainstorms when the slope is 0.0005 and 0.01, the subsurface is homogeneous, and a no-flow bottom BC is applied. Even though a single soil profile was employed in the coupled H1D-K2 model, the hydrograph shapes were very similar for both models. The only discrepancy was in the cumulative runoff for relatively flat (0.0005) and steep (0.01) slopes was only 0.14 % and 0.22 %, respectively (Table S1). There was also a slight difference (less than 5.0×10^{-5} m^2/s) in peak outflow during the second rainfall event (t = 200–400 mins). Similarly, the simulated water depths by the coupled H1D-K2 model were in good agreement with those obtained by the H2D model at the three observation points (Fig. 9b and 9c for slopes of 0.0005 and 0.01, respectively). Furthermore, the timing of the predicted onset and cessation of surface runoff were the same for all surface points using the coupled H1D-K2 and H2D models (Fig. 9c). The biggest difference in ponding depths between the two models was observed during the second rainfall event (about 1 mm) because H2D predicts ponding at the lower part of the hillslope.

4.3.2. *Free drainage bottom BC*

Fig. 10 illustrates that the coupled H1D-K2 model reproduced similar hydrographs to the H2D model for homogeneous hillslopes with a free drainage bottom BC subjected to multiple rainstorms. The free drainage BC causes dryer soil conditions and facilitates surface water infiltration compared to a no-flow bottom BC. The free drainage BC resulted in decreased peak amplitudes of surface runoff for all rainfall events (Fig. 10a) compared to the no-flow BC (Fig. 9a). During the low-intensity rainfall ($0 < q_r < K_s$), the outflow rate decreased gradually. The second wave of surface runoff (present in the previous example due to saturation excess) did not occur because the subsurface storage was not entirely filled due to the continued draining of the subsurface.

Fig. 10b shows the temporal evolution of the surface water depth at observation points h_1, h_2, and h_3. While the results simulated by the H1D-K2 model agree closely with the H2D model's results for all test cases, there was a small difference in the timing of surface runoff cessation. The water depth at the three observation points decreased to zero simultaneously in the H1D-K2 model, whereas they gradually and successively dropped to zero in the H2D model.

5. Discussion

The H2D and coupled H1D-K2 models predict similar hydrological behaviors at the land surface and in the subsurface of homogeneous and heterogeneous hillslopes subject to a uniform rainfall (Figs. 4, 5, and 7) or multiple rainstorms (Figs. 9 and 10). The simulated components of the water balance are very close to each other (Tables 2, 3, and S1). Discrepancies in the onset and cessation of surface runoff and spatial and temporal water content distributions simulated by the two models are caused mainly by the coupling strategy, the time interval Δt_p, and the number of the H1D soil profiles (nh1d).

First, the coupled H1D-K2 model uses the BC switching approach to execute the two codes sequentially. This results in the subsurface flow equation being solved before the surface flow equation, with subsurface flow affecting surface flow at the current time level while surface flow affecting subsurface flow only at the next time level.

Second, the fixed Δt_p also contributes to discrepancies because of a time lag in updating BCs. The H1D model calculates the actual infiltration rate with applied surface conditions obtained at the end of the previous period (Fig. 2). Although water inflows and outflows are

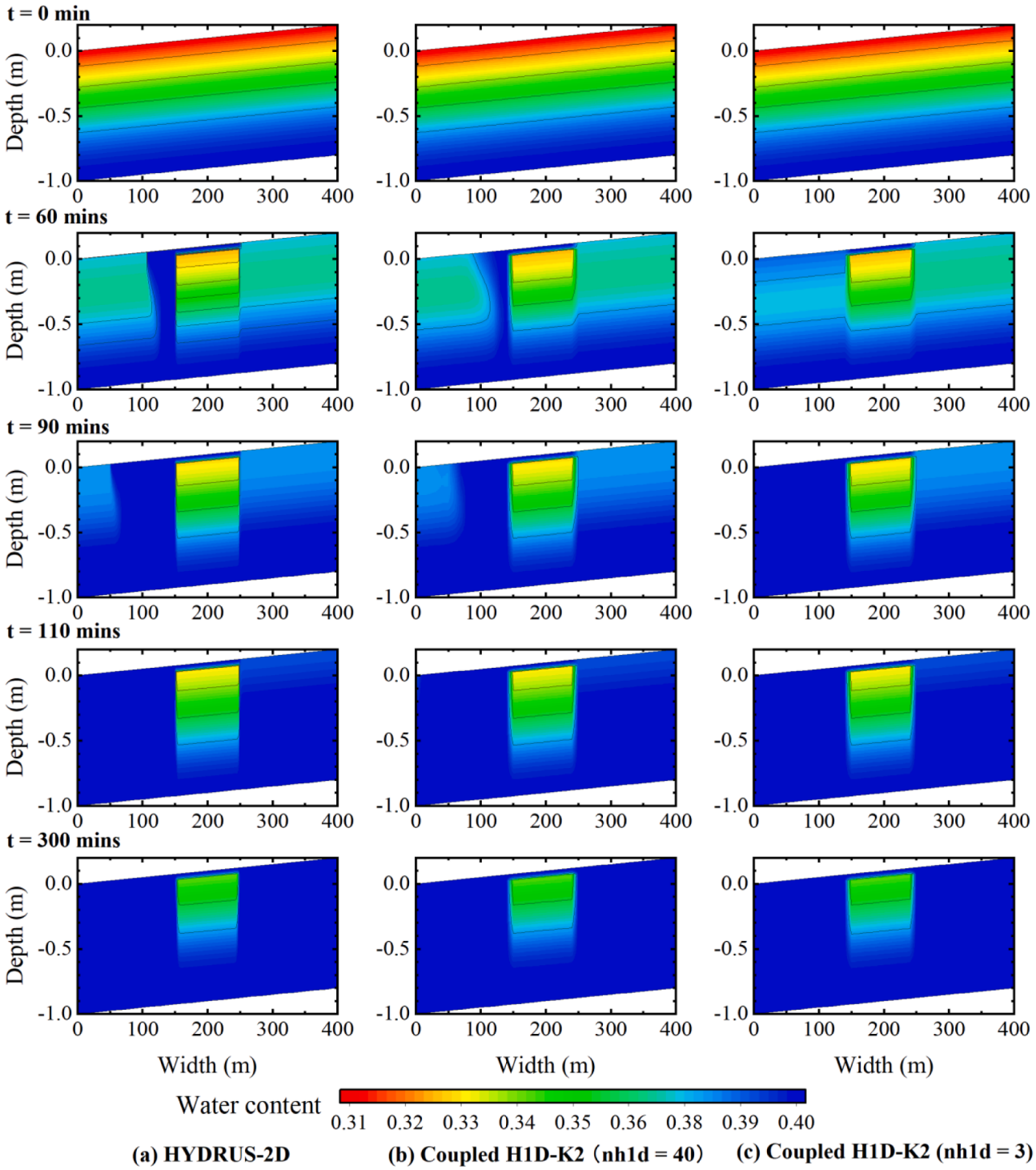

Fig. 8. Simulated water content distributions for heterogeneous case 2 with a no-flow bottom BC at times of 0, 60, 90, 110, and 300 mins (top to bottom) simulated by H2D (left), coupled H1D-K2 with 40 soil profiles (middle), and coupled H1D-K2 with three soil profiles (right). The vertical distance is not at scale. nh1d is the number of the H1D soil profiles.

balanced during particular time steps of the simulation, the time-lagged approach may cause uncertainty in the distribution of net surface fluxes in surface nodes (Eq. (5)), which eventually affects the accuracy of the simulated results. Despite adopting the same sequential solution procedure, the H2D model updates BCs in each individual time step, which is much smaller than Δt_p. This is the main reason for discrepancies in the simulated outflow rate between two models (Fig. 5a and S3). Similar conclusions about the limitation of this time-lagged approach have been discussed in the literature (e.g., Panday and Huyakorn, 2004, Huang and Yeh, 2009).

Third, the number of H1D soil profiles causes discrepancies in spatial and temporal water content distributions (Figs. 6 and 8), onset of the second outflow wave, and the surface water flow depths (Fig. 5b and 7). When only one H1D soil profile is used to represent the entire subsurface, the volume of infiltrated water contributed by ponding at multiple surface nodes is redistributed to one soil profile. This process causes higher water contents at an earlier stage (Fig. S1c and S2c) and delays soil saturation (Fig. S1e and S2e). Water fluxes at multiple surface nodes

Table 3
Mass balance components simulated by the coupled H1D-K2 and H2D models for heterogeneous case 2 with a slope of 0.01 and a no-flow BC applied at the bottom.

	Cum. precip. (m^2)	Cum. outflow (m^2)	Surface storage (m^2)	Subsurface storge (m^2)	Relative MBE (%)	Onset of outflow (mins)	Peak flow (m^2/s)	Comp. time (s)
H2D	26.40	12.65	0.68	13.35	0.54	108.3	2.08×10^{-3}	24.35
H1D-K2 (nh1d* = 40)	26.40	12.69	0.70	13.44	1.64	103.0	2.10×10^{-3}	145.92
H1D-K2 (nh1d* = 3)	26.40	12.65	0.70	13.45	1.50	91.0	2.10×10^{-3}	16.71

Note: *nh1d – the number of the H1D soil profiles.

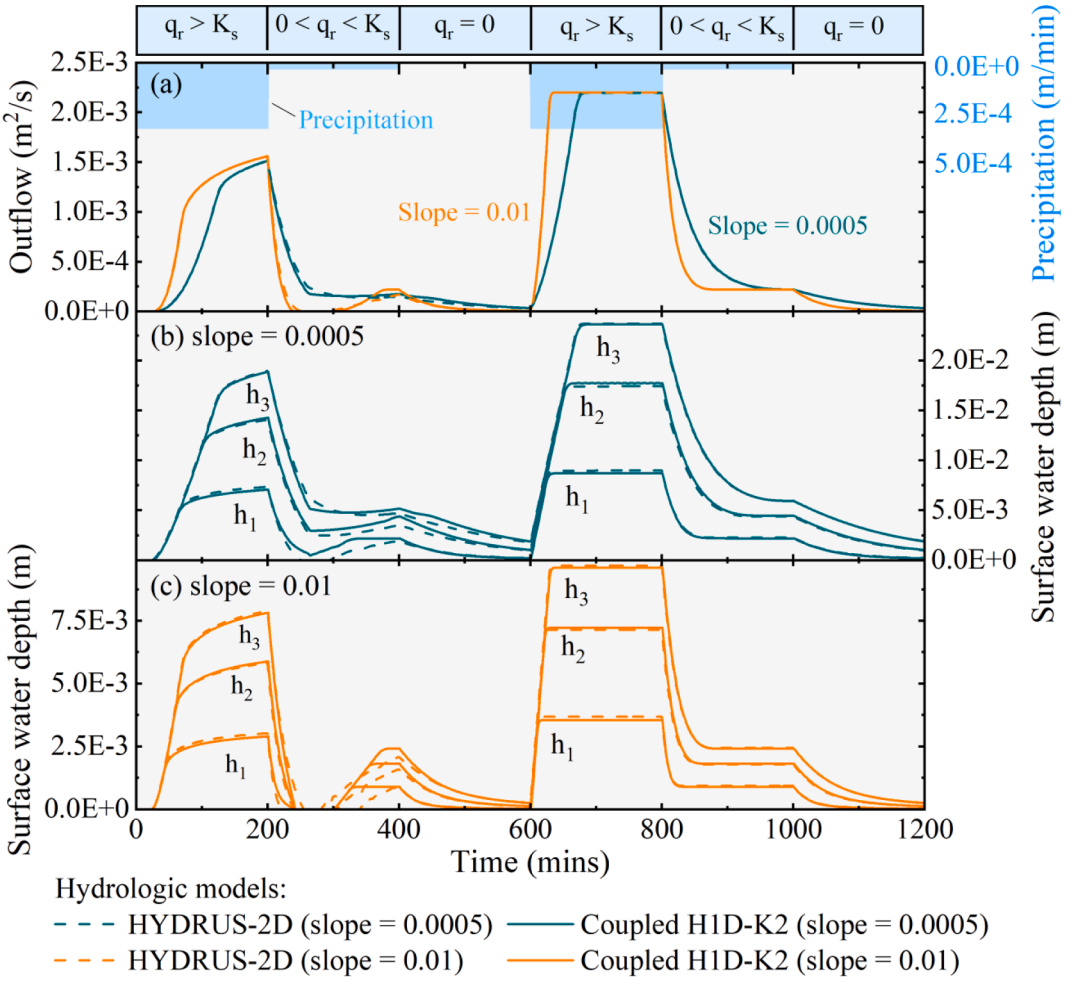

Fig. 9. (a) Comparison of outflow rates for the homogeneous hillslopes with a no-flow BC and a slope of 0.0005 and 0.01 simulated by the H2D (dash lines) and coupled H1D-K2 (solid lines) models; (b) simulated surface water depths for the hillslope with a slope of 0.0005; and (c) simulated surface water depths for the hillslope with a slope of 0.01. h_1, h_2, and h_3 are three observation points located at 320 m (uphill), 260 m (middle), and 0 m (downhill) away from the outlet, respectively.

are also applied to only one soil profile (Eq. (5)), causing ponding (Fig. 9) or infiltration (Fig. 10), in all nodes.

Furthermore, differences between H1D-K2 and H2D models for a homogeneous hillslope (Fig. 4) were much smaller than for the heterogeneous hillslope (Figs. 5 and 7). The main reason is that the direction of unsaturated water flow in a homogeneous hillslope is predominantly vertical, and water starts ponding on the entire plane at the same time. Also, a relatively small surface flow depth (a maximum of 3.0 cm) does not significantly impact the infiltration rate (Fig. S4), resulting in a nearly uniform infiltration rate along the homogeneous hillslope. This indicates that one H1D soil profile is sufficient to accurately simulate water flow in the homogeneous hillslopes. Previous studies have reported similar conclusions (e.g., Smith and Woolhiser, 1971, Singh and Bhallamudi, 1998). On the other hand, the H1D-K2 model with three soil profiles only broadly approximates the movement of the surface-water front at a heterogeneous hillslope (Figs. 6 and 8). The H1D-K2 model can fully capture (similarly to H2D) the general behavior of heterogeneous hillslopes when more vertical H1D soil profiles are employed (Fig. 6b and 8b). When users do not need accurate spatial moisture distribution (Figs. 6 and 8), it is better to use the H1D-K2 model due to the higher computational efficiency.

The simulation results of the H1D-K2 model also agree closely with those presented in an integrated hydrologic model intercomparison project (Maxwell et al., 2014). In this project, seven broadly used integrated hydrologic models were compared, including ATS (Coon et al., 2020), CATHY (Sulis et al., 2010), HydroGeoSphere (Brunner and

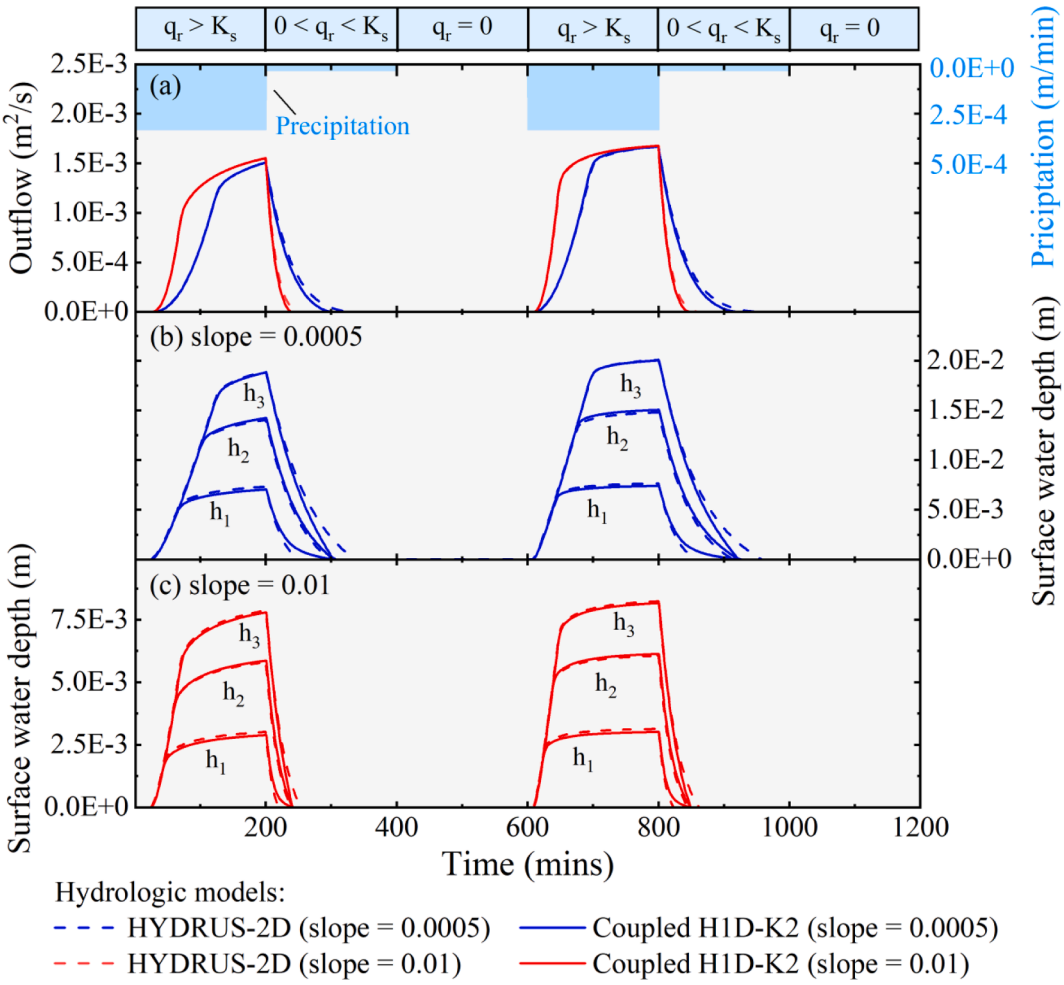

Fig. 10. (a) Comparison of outflow rates for the homogeneous hillslopes with a free drainage BC and a slope of 0.0005 and 0.01 simulated by the HYDRUS-2D (dash lines) and coupled H1D-K2 (solid lines) models; (b) simulated surface water depths for the hillslope with a slope of 0.0005; and (c) simulated surface water depths for the hillslope with a slope of 0.01. h_1, h_2, and h_3 are three observation points located at 320 m (uphill), 260 m (middle), and 0 m (downhill) away from the outlet, respectively.

Simmons, 2012), MIKE SHE (Thompson et al., 2004), and ParFlow (Kollet and Maxwell, 2006). For the homogeneous cases (infiltration excess and saturation excess, Fig. 4), the peak flow and the onset of flow are almost identical to the results obtained by the seven integrated hydrologic models (Maxwell et al., 2014). For heterogeneous case 2 (Fig. 7 and Table 3), the peak flow (mean relative error of 7.1 % with a deviation of 4.8 %) and the onset of flow (mean value of 17.7 % with a deviation of 13.4 %) fell within the range of results presented in Maxwell et al. (2014). Similar to our findings, these discrepancies have mainly been attributed to differences in the coupling strategy, Δt_p, and the number of soil profiles (Huang and Yeh, 2009, Sulis et al., 2010, Maxwell et al., 2014).

Compared to H2D, the H1D-K2 code can reduce the computational time (Tables 2, 3, and S1) because the dimensionality reduction decreases the number of elements and nodes for calculation. The BC switching approach allows surface and subsurface flow equations to be separately solved using dynamic time steps (Fig. 1), which overcomes numerical instabilities of subsurface solutions caused by fast surface flow. Our approach calculates infiltration rates for the entire plane when ponding occurs using the average surface water depth (Eq. (4)) and rearranges the net surface flux to surface nodes based on individual surface water depths (Eq. (5)). Similarly, Singh and Bhallamudi (1998) demonstrated up to 10 times speedup when using a uniform infiltration rate compared to a non-uniform infiltration rate at surface nodes.

The surface flow on a hillslope can be represented by a cascade of 1D overland flow planes, while the subsurface flow is assumed to occur only in the vertical direction. Our water balance and BC switching approach enables the H1D-K2 model to accurately consider the feedback of subsurface processes (e.g., evaporation, infiltration, drainage) on surface water flow. Furthermore, by replacing the empirical infiltration equation in the K2 model with a physically based H1D model, the H1D-K2 model can overcome the limitation of predicting the surface runoff generated by the saturation excess conditions (Fig. S5) and can provide spatial and temporal water content distributions (Figs. 6, 8, S1, and S2). The H1D-K2 model can consider multiple soil layers with different soil textures, whereas the standard K2 model can only consider two-soil layers, while the lower layer must be infinite. Spatial variations in the subsoil characteristics in the vertical direction can be accurately captured by the H1D-K2 model, which presently does not account for lateral water flow in the vadose zone.

Note that MATLAB only serves as a platform to exchange information between the H1D and K2 codes and assignes exchange fluxes to separate surface and subsurface nodes based on the surface water depth. When access to a comprehensive set of MATLAB and Simulink products is restricted, one could use other programming languages (e.g., R, Python, C++, etc.) to create the coupling routine with the same structure and the spatial and temporal loops described in section 2.1 and Fig. 2. Our external coupling approach keeps two codes independent, allowing users to use their latest versions in the coupled H1D-K2 code. Another advantage of this approach is the ease of parallel computing

implementation since hydrological processes in an H1D soil profile are independent of other soil profiles. Furthermore, the users can also run the coupled H1D-K2 code on high-performance computing cluster systems after integrating with the MATLAB Parallel Server.

However, the main advantage of the H1D-K2 model compared to K2 is that it can consider complex meteorological conditions (rainfall variability), different soil textures, different initial water conditions, different bottom BCs (e.g., free drainage, seepage face, variable fluxes/pressures), and the effects of vegetation, which are the dominant factors for subsurface flow conditions. Moreover, since the physical nonequilibrium flow model (e.g., dual-porosity and dual-permeability) has been developed in the computational module of H1D (Simunek et al., 2005), the same conceptualization can be used in the coupled H1D-K2 model to simulate the impacts of physical nonequilibrium on surface water flow. Future research will extend this computationally efficient model to a watershed scale by dividing the domain into a cascade of overland flow planes and channels.

6. Conclusions

A novel approach was developed to couple open-source codes for vadose zone flow (HYDRUS-1D) and overland flow (KINEROS2), resulting in the H1D-K2 model. This new coupling routine sequentially solved the Richards equation for subsurface flow and the kinematic wave equation for overland flow. A water balance and BC switching approach was used to couple the surface and subsurface hydrological processes. The water exchange flux in an H1D profile was assigned to multiple surface nodes in the K2 calculation using a weighting factor related to the water depth.

Six benchmark problems were performed over a wide range of conditions with different saturated hydraulic conductivities, initial conditions, bottom BCs, slopes, and multiple rainstorm events. The simulated hydrographs, surface water depth, and water components by the coupled H1D-K2 model closely agree with those obtained by the H2D model. The coupled H1D-K2 model is a simple, accurate, and computationally efficient hydrologic model. It can simulate surface runoff generated by infiltration excess and saturation excess in response to rainfall or inflow. It can also provide spatial and temporal water content distributions and surface water depths. Its computational efficiency is improved by adopting a dynamic time step approach and applying one H1D soil profile to an entire overland flow plane rather than to individual surface nodes. A heterogeneous hillslope can be divided into a cascade of planes with different slopes, spatial variations of soil characteristics, and different drainage conditions at the bottom. The novel coupling approach and the H1D-K2 model can be extended to larger scales by dividing a watershed into a cascade of overland flow planes and implementing parallel computing to improve computational efficiency.

CRediT authorship contribution statement

Lin Chen: Conceptualization, Formal analysis, Methodology, Software, Writing – original draft, Visualization. **Jiří Šimůnek:** Conceptualization, Funding acquisition, Supervision, Project administration, Writing – review & editing. **Scott A. Bradford:** Conceptualization, Funding acquisition, Supervision, Project administration, Writing – review & editing. **Hoori Ajami:** Conceptualization, Funding acquisition, Supervision, Project administration, Writing – review & editing. **Menberu B. Meles:** Conceptualization, Writing – review & editing.

Declaration of Competing Interest

The authors declare that they have no known competing financial interests or personal relationships that could have appeared to influence the work reported in this paper.

Data availability

Data will be made available on request.

Acknowledgements

This research was supported by the United States Department of Agriculture, Agricultural Research Service, National Program 211. The authors thank Prof. Carl L. Unkrich (USDA-ARS, Tucson, AZ) for providing insightful comments and suggestions for the modification of the KINEROS2 code.

Open research

The HYDRUS-1D software is publicly available on the PC-Progress website; its standard computational module is open source (https://www.pc-progress.com/en/Default.aspx?hydrus-1d). The KINEROS2 model is also open-source and available on https://www.tucson.ars.ag.gov/kineros/. A HYDRUS (2D/3D) license would be required to run the HYDRUS-2D model. The MATLAB script is available by contacting Dr. Lin Chen (linc@ucr.edu, chl_sc@163.com).

Appendix A. Supplementary data

Supplementary data to this article can be found online at https://doi.org/10.1016/j.jhydrol.2022.128539.

References

Abbott, M.B., Bathurst, J.C., Cunge, J.A., O'Connell, P.E., Rasmussen, J., 1986. An introduction to the European Hydrological System — Systeme Hydrologique European, "SHE", 2: Structure of a physically-based, distributed modelling system. J. Hydrol. 87 (1), 61–77. https://doi.org/10.1016/0022-1694(86)90115-0.

Beegum, S., Simunek, J., Szymkiewicz, A., Sudheer, K., Nambi, I.M., 2018. Updating the coupling algorithm between HYDRUS and MODFLOW in the HYDRUS package for MODFLOW. Vadose Zone J. 17 (1), 180034. https://doi.org/10.2136/vzj2018.02.0034.

Brunetti, G., Simunek, J., Bautista, E., 2018. A hybrid finite volume-finite element model for the numerical analysis of furrow irrigation and fertigation. Comput. Electron. Agric. 150, 312–327. https://doi.org/10.1016/j.compag.2018.05.013.

Brunner, P., Simmons, C.T., 2012. HydroGeoSphere: a fully integrated, physically based hydrological model. Groundwater 50 (2), 170–176. https://doi.org/10.1111/j.1745-6584.2011.00882.x.

Camporese, M., Paniconi, C., Putti, M., Orlandini, S., 2010. Surface-subsurface flow modeling with path-based runoff routing, boundary condition-based coupling, and assimilation of multisource observation data. Water Resour. Res. 46 (W02512) https://doi.org/10.1029/2008WR007536.

Camporese, M., Daly, E., Dresel, P.E., Webb, J.A., 2014. Simplified modeling of catchment-scale evapotranspiration via boundary condition switching. Adv. Water Resour. 69, 95–105. https://doi.org/10.1016/j.advwatres.2014.04.008.

Coon, E.T., Moulton, J.D., Kikinzon, E., Berndt, M., Manzini, G., Garimella, R., Painter, S. L., 2020. Coupling surface flow and subsurface flow in complex soil structures using mimetic finite differences. Adv. Water Resour. 144, 103701 https://doi.org/10.1016/j.advwatres.2020.103701.

De Maet, T., Cornaton, F., Hanert, E., 2015. A scalable coupled surface–subsurface flow model. Comput. Fluids 116, 74–87. https://doi.org/10.1016/j.compfluid.2015.03.028.

Ebel, B.A., Mirus, B.B., Heppner, C.S., VanderKwaak, J.E., Loague, K., 2009. First-order exchange coefficient coupling for simulating surface water–groundwater interactions: parameter sensitivity and consistency with a physics-based approach. Hydrol. Process. 23 (13), 1949–1959. https://doi.org/10.1002/hyp.7279.

Fan, Y., Clark, M., Lawrence, D.M., Swenson, S., Band, L., Brantley, S.L., Grant, G., 2019. Hillslope hydrology in global change research and Earth system modeling. Water Resour. Res. 55 (2), 1737–1772. https://doi.org/10.1029/2018WR023903.

Fatichi, S., Vivoni, E.R., Ogden, F.L., Ivanov, V.Y., Mirus, B., Gochis, D., Tarboton, D., 2016. An overview of current applications, challenges, and future trends in distributed process-based models in hydrology. J. Hydrol. 537, 45–60. https://doi.org/10.1016/j.jhydrol.2016.03.026.

Freeze, R.A., 1972. Role of subsurface flow in generating surface runoff: 2. Upstream source areas. Water Resour. Res. 8 (5), 1272–1283. https://doi.org/10.1029/WR008i005p01272.

Giráldez, J., Woolhiser, D., 1996. Analytical integration of the kinematic equation for runoff on a plane under constant rainfall rate and Smith and Parlange infiltration. Water Resour. Res. 32 (11), 3385–3389.

Goodrich, D., Burns, I., Unkrich, C., Semmens, D.J., Guertin, D., Hernandez, M., Levick, L.R., 2012. KINEROS2/AGWA: model use, calibration, and validation. Trans. ASABE 55 (4), 1561–1574.

Goodrich, D.C., Unkrich, C.L,. Smith, R.E., Woolhiser, D.A., 2006. KINEROS2-new features and capabilities. Proceedings of the Joint Federal Interagency Conference: April 2-6, 2006, Reno, NV: proceedings of the 3rd Federal Hydrologic Modeling Conference: proceedings of the 8th Federal Interagency Sedimentation Conference, [Sl]: Subcommittee on Hydrology, 2006.

Gottardi, G., Venutelli, M., 1993. A control-volume finite-element model for two-dimensional overland flow. Adv. Water Resour. 16 (5), 277–284. https://doi.org/10.1016/0309-1708(93)90019-C.

Guber, A.K., Pachepsky, Y.A., Yakirevich, A.M., Shelton, D.R., Whelan, G., Goodrich, D. C., Unkrich, C.L., 2014. Modeling runoff and microbial overland transport with KINEROS2/STWIR model: Accuracy and uncertainty as affected by source of infiltration parameters. J. Hydrol. 519, 644–655. https://doi.org/10.1016/j.jhydrol.2014.08.005.

Haddeland, I., Heinke, J., Biemans, H., Eisner, S., Flörke, M., Hanasaki, N., Konzmann, M., Ludwig, F., Masaki, Y., Schewe, J., Stacke, T., Tessler, Z.D., Wada, Y., Wisser, D., 2014. Global water resources affected by human interventions and climate change. PNAS 111 (9), 3251–3256.

He, Z., Wu, W., Wang, S.S., 2008. Coupled finite-volume model for 2D surface and 3D subsurface flows. J. Hydrol. Eng. 13 (9), 835–845. https://doi.org/10.1061/(ASCE)1084-0699(2008)13:9(835).

Huang, G., Yeh, G.-T., 2009. Comparative study of coupling approaches for surface water and subsurface interactions. J. Hydrol. Eng. 14 (5), 453–462. https://doi.org/10.1061/(ASCE)HE.1943-5584.0000017.

Jaber, F.H., Mohtar, R.H., 2003. Stability and accuracy of two-dimensional kinematic wave overland flow modeling. Adv. Water Resour. 26 (11), 1189–1198. https://doi.org/10.1016/S0309-1708(03)00102-7.

Köhne, J.M., Wöhling, T., Pot, V., Benoit, P., Leguédois, S., Le Bissonnais, Y., Simunek, J., 2011. Coupled simulation of surface runoff and soil water flow using multi-objective parameter estimation. J. Hydrol. 403 (1–2), 141–156. https://doi.org/10.1016/j.jhydrol.2011.04.001.

Kollet, S.J., Maxwell, R.M., 2006. Integrated surface–groundwater flow modeling: A free-surface overland flow boundary condition in a parallel groundwater flow model. Adv. Water Resour. 29 (7), 945–958. https://doi.org/10.1016/j.advwatres.2005.08.006.

Kollet, S., Sulis, M., Maxwell, R.M., Paniconi, C., Putti, M., Bertoldi, G., Sudicky, E., 2017. The integrated hydrologic model intercomparison project, IH-MIP2: A second set of benchmark results to diagnose integrated hydrology and feedbacks. Water Resour. Res. 53 (1), 867–890. https://doi.org/10.1002/2016WR019191.

Kourakos, G., Dahlke, H.E., Harter, T., 2019. Increasing groundwater availability and seasonal base flow through agricultural managed aquifer recharge in an irrigated basin. Water Resour. Res. 55 (9), 7464–7492. https://doi.org/10.1029/2018WR024019.

Lawrence, D.M., Fisher, R.A., Koven, C.D., Oleson, K.W., Swenson, S.C., Bonan, G., Zeng, X., 2019. The community land model version 5: description of new features, benchmarking, and impact of forcing uncertainty. J. Adv. Model. Earth Syst. 11 (12), 4245–4287. https://doi.org/10.1029/2018MS001583.

Liggett, J.E., Werner, A.D., Simmons, C.T., 2012. Influence of the first-order exchange coefficient on simulation of coupled surface–subsurface flow. J. Hydrol. 414–415, 503–515. https://doi.org/10.1016/j.jhydrol.2011.11.028.

Mantoglou, A., 1992. A theoretical approach for modeling unsaturated flow in spatially variable soils: Effective flow models in finite domains and nonstationarity. Water Resour. Res. 28 (1), 251–267. https://doi.org/10.1029/91WR02232.

Marwaha, N., G. Kourakos, Levintal, E., Dahlke, H.E., 2021. Identifying agricultural managed aquifer recharge locations to benefit drinking water supply in rural communities. Water Resour. Res. 57(3): e2020WR028811. 10.1029/2020WR028811.

Maxwell, R.M., Putti, M., Meyerhoff, S., Delfs, J.-O., Ferguson, I.M., Ivanov, V., Sulis, M., 2014. Surface-subsurface model intercomparison: A first set of benchmark results to diagnose integrated hydrology and feedbacks. Water Resour. Res. 50 (2), 1531–1549. https://doi.org/10.1002/2013WR013725.

Meles Bitew, M., Jackson, C.R., Goodrich, D.C., Younger, S.E., Griffiths, N.A., Vaché, K. B., Rau, B., 2020. Dynamic domain kinematic modelling for predicting interflow over leaky impeding layers. Hydrol. Process. 34 (13), 2895–2910. https://doi.org/10.1002/hyp.13778.

Morita, M., Yen, B.C., 2002. Modeling of conjunctive two-dimensional surface-three-dimensional subsurface flows. J. Hydraul. Eng. 128 (2), 184–200. https://doi.org/10.1061/(ASCE)0733-9429(2002)128:2(184).

Niswonger, R.G., Prudic, D.E., Regan, R.S., 2006. Documentation of the unsaturated-zone flow (UZF1). Package for Modeling Unsaturated Flow Between the Land Surface and the Water Table With MODFLOW-2005.

Niswonger, R.G., Morway, E.D., Triana, E., Huntington, J.L., 2017. Managed aquifer recharge through off-season irrigation in agricultural regions. Water Resour. Res. 53 (8), 6970–6992. https://doi.org/10.1002/2017WR020458.

Orth, R., Staudinger, M., Seneviratne, S.I., Seibert, J., Zappa, M., 2015. Does model performance improve with complexity? A case study with three hydrological models. J. Hydrol. 523, 147–159. https://doi.org/10.1016/j.jhydrol.2015.01.044.

Panday, S., Huyakorn, P.S., 2004. A fully coupled physically-based spatially-distributed model for evaluating surface/subsurface flow. Adv. Water Resour. 27 (4), 361–382. https://doi.org/10.1016/j.advwatres.2004.02.016.

Parlange, J.-Y., Lisle, I., Braddock, R., Smith, R., 1982. The three-parameter infiltration equation. Soil Sci. 133 (6), 337–341.

Qu, Y., Duffy, C.J., 2007. A semidiscrete finite volume formulation for multiprocess watershed simulation. Water Resour. Res. 43 (W08419) https://doi.org/10.1029/2006WR005752.

Report, U. W. W. D. (2018). 2018 UN World Water Development Report, Nature-based Solutions for Water, www.unwater.org/publications/world-water-development-report-2018/. United Nations Educational, Scientific and Cultural Organization, New York, United States.

Roberts, A., 2003. A holistic finite difference approach models linear dynamics consistently. Math. Comput. 72 (241), 247–262. https://doi.org/10.1090/S0025-5718-02-01448-5.

Sasidharan, S., Bradford, S.A., Simunek, J., DeJong, B., Kraemer, S.R., 2018. Evaluating drywells for stormwater management and enhanced aquifer recharge. Adv. Water Resour. 116, 167–177. https://doi.org/10.1016/j.advwatres.2018.04.003.

Seo, H.S., Šimůnek, J., Poeter, E.P., 2007. Documentation of the HYDRUS package for MODFLOW-2000, the US geological survey modular ground-water model. IGWMC-International Ground Water Modeling Center.

Šimůnek, J., 2015. Implementation of Overland Flow into HYDRUS (2D/3D), HYDRUS Software Series 6b. Department of Environmental Sciences, University of California Riverside, Riverside, CA, 44 pp., May 2015.

Simunek, J., van Genuchten, M.T., Šejna, M., 2016. Recent developments and applications of the HYDRUS computer software packages. Vadose Zone J. 15 (7), 25. https://doi.org/10.2136/vzj2016.04.0033.

Šimůnek, J., Van Genuchten, M. T., Šejna, M., 2006. The HYDRUS software package for simulating two- and three-dimensional movement of water, heat, and multiple solutes in variably-saturated media. Technical manual, version 1: 241.

Šimůnek, J., 2003. HYDRUS-2D Code Modification: Modeling Overland Flow and Dynamic Interactions Between Plants and Water Flow in a Hillslope Transect. Idaho National Environmental Laboratory, Final report for project under contract: 55.

Šimunek, J., van Genuchten, M.T., 2008. Modeling nonequilibrium flow and transport processes using HYDRUS. Vadose Zone J. 7 (2), 782–797. https://doi.org/10.2136/vzj2007.0074.

Šimunek, J., Van Genuchten, M.T., Sejna, M., 2005. The HYDRUS-1D software package for simulating the one-dimensional movement of water, heat, and multiple solutes in variably-saturated media. Univ. California-Riverside Res. Rep. 3, 1–240.

Singh, V., Bhallamudi, S.M., 1998. Conjunctive surface-subsurface modeling of overland flow. Adv. Water Resour. 21 (7), 567–579. https://doi.org/10.1016/S0309-1708(97)00020-1.

Singh, V.P., Woolhiser, D.A., 2002. Mathematical modeling of watershed hydrology. J. Hydrol. Eng. 7 (4), 270–292. https://doi.org/10.1061/(ASCE)1084-0699(2002)7:4(270).

Smith, R.E., Goodrich, D.C., Unkrich, C.L., 1999. Simulation of selected events on the Catsop catchment by KINEROS2: a report for the GCTE conference on catchment scale erosion models. CATENA 37 (3), 457–475. https://doi.org/10.1016/S0341-8162(99)00033-8.

Smith, R.E., Hebbert, R.H.B., 1983. Mathematical simulation of interdependent surface and subsurface hydrologic processes. Water Resour. Res. 19 (4), 987–1001. https://doi.org/10.1029/WR019i004p00987.

Smith, M.B., Seo, D.-J., Koren, V.I., Reed, S.M., Zhang, Z., Duan, Q., Cong, S., 2004. The distributed model intercomparison project (DMIP): motivation and experiment design. J. Hydrol. 298 (1), 4–26. https://doi.org/10.1016/j.jhydrol.2004.03.040.

Smith, M.B., Koren, V., Reed, S., Zhang, Z., Zhang, Y., Moreda, F., Cosgrove, B.A., 2012. The distributed model intercomparison project – Phase 2: Motivation and design of the Oklahoma experiments. J. Hydrol. 418–419, 3–16. https://doi.org/10.1016/j.jhydrol.2011.08.055.

Smith, R.E., Woolhiser, D.A., 1971. Overland flow on an infiltrating surface. Water Resour. Res. 7 (4), 899–913. https://doi.org/10.1029/WR007i004p00899.

Sulis, M., Meyerhoff, S.B., Paniconi, C., Maxwell, R.M., Putti, M., Kollet, S.J., 2010. A comparison of two physics-based numerical models for simulating surface water–groundwater interactions. Adv. Water Resour. 33 (4), 456–467. https://doi.org/10.1016/j.advwatres.2010.01.010.

Thompson, J., Sørenson, H.R., Gavin, H., Refsgaard, A., 2004. Application of the coupled MIKE SHE/MIKE 11 modelling system to a lowland wet grassland in southeast England. J. Hydrol. 293 (1–4), 151–179. https://doi.org/10.1016/j.jhydrol.2004.01.017.

van Genuchten, M.T., 1980. A closed-form equation for predicting the hydraulic conductivity of unsaturated soils. Soil Sci. Soc. Am. J. 44 (5), 892–898. https://doi.org/10.2136/sssaj1980.03615995004400050002x.

Vorosmarty, C.J., Green, P., Salisbury, J., Lammers, R.B., 2000. Global water resources: vulnerability from climate change and population growth. Science 289 (5477), 284–288. https://doi.org/10.1126/science.289.5477.284.

Wang, D., Liu, Y., Kumar, M., 2018. Using nested discretization for a detailed yet computationally efficient simulation of local hydrology in a distributed hydrologic model. Sci. Rep. 8, 5785. https://doi.org/10.1038/s41598-018-24122-7.

Wen, H., Brantley, S.L., Davis, K.J., Duncan, J.M., Li, L., 2021. The Limits of homogenization: what hydrological dynamics can a simple model represent at the catchment scale? Water Resour. Res. 57 (6) https://doi.org/10.1029/2020WR029528 e2020WR029528.

Woolhiser, D., Hanson, C., Kuhlman, A., 1970. Overland flow on rangeland watersheds. J. Hydrol. 9 (2), 336–356.

Woolhiser, D.A., Liggett, J.A., 1967. Unsteady, one-dimensional flow over a plane—the rising hydrograph. Water Resour. Res. 3 (3), 753–771. https://doi.org/10.1029/WR003i003p00753.